Journal of Sol-Gel Science and Technology (2019) 92:449–457
https://doi.org/10.1007/s10971-019-04974-9

ORIGINAL PAPER: SOL-GEL, HYBRIDS AND SOLUTION CHEMISTRIES

Check for updates

Synthesis and properties of carbon–metal oxide nanomaterials

Anastasiya G. Navrotskaya[1] · Elena F. Krivoshapkina[1,2] · Igor A. Perovskiy[3] · Yuri I. Bauman[4] · Ilya V. Mishakov[4] · Aleksey A. Vedyagin[4] · Sergey I. Isaenko[3] · Pavel V. Krivoshapkin[1,2]

Received: 21 December 2018 / Accepted: 16 March 2019 / Published online: 31 March 2019

Abstract

In this paper, the sorption of the heavy metal ions (Sr^{2+}, Ba^{2+}, and Cs^{+}) on the hybrid CNF/TiO_2 and CNF/Fe_2O_3 materials is considered. The colloid–chemical properties of the TiO_2 and Fe_2O_3 nanoparticles and carbon nanofibers in the dispersions were studied, and interaction between nanoparticles and nanofibers in accordance with the hetero-coagulation principle was estimated. The carbon nanofibers used were prepared by catalytic chemical vapor deposition of a propane–butane mixture over the nickel–copper catalyst and then functionalized by boiling in a mixture of concentrated hydrochloric and nitric acids. The TiO_2 and Fe_2O_3 nanoparticles were synthesized via a sol–gel technique. The sol was mixed with carbon nanofibers. After drying, the hybrid materials with a uniform distribution of the oxide NPs along the nanofiber's surface were obtained. The CNF-to-metal oxide ratios were 10:1 and 1:1. The samples were characterized by a set of physicochemical methods. The hybrid CNF/TiO_2 system was found to have a synergetic effect toward the sorption of the metal ions from their aqueous solutions.

Graphical Abstract

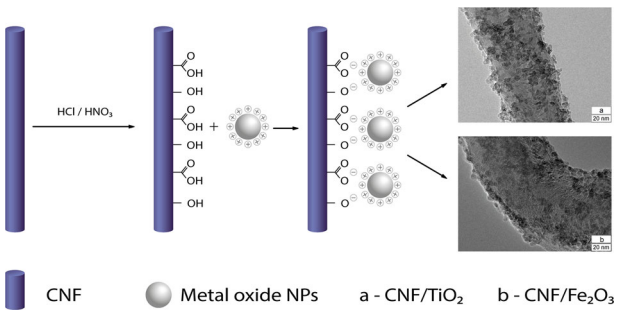

Highlights

- Hybrid materials CNF/Fe_2O_3 and CNF/TiO_2 were synthesized by ex situ method.
- The colloid–chemical properties of metal oxide NPs and CNFs in the dispersions were studied.
- Metal oxide NPs are coaxially coated and uniformly distributed on the CNF surface.
- Sorption of Sr^{2+}, Ba^{2+}, and Cs^{+} on the hybrid materials is considered.
- The hybrid CNF/TiO_2 was found to have a synergetic effect toward the sorption of Sr^{2+} and Cs^{+}.

Keywords Carbon nanofibers · Fe_2O_3 · TiO_2 · Hybrids · Extraction

✉ Pavel V. Krivoshapkin
chemicalpasha@mail.ru

[1] ITMO University, St. Petersburg 197101, Russia

[2] Institute of Chemistry of Federal Research Centre "Komi Science Centre of the Ural Branch of the Russian Academy of Sciences", Syktyvkar 167982, Russia

[3] Institute of Geology of Federal Research Centre "Komi Science Centre of the Ural Branch of the Russian Academy of Sciences", Syktyvkar 167982, Russia

[4] Boreskov Institute of Catalysis, Siberian Branch, Russian Academy of Sciences, Novosibirsk 630090, Russia

1 Introduction

Creation of the hybrid materials based on nanostructured carbon is an excellent investment in development of the future functional materials. There are several types of carbon-based nanomaterials that have different structures and properties. The first of them are nanocomposites, which contain a filler (carbon) and a matrix or base (e.g., ceramic or polymer) and which usually combine the individual properties of both compounds [1]. Unlike nanocomposites, carbon hybrid nanomaterials provide access to a large specific surface area and an extended interface. Due to this morphology, charge and energy transfer processes create synergistic effects that lead to unique physicochemical properties and increased productivity [2, 3].

Hybrid carbon nanomaterials are intensively researched and applied in various areas of nanotechnology, such as environmental catalysis, photocatalysis, sensors, batteries, and photovoltaics [2, 3]. One of the most promising areas for application of these materials is adsorption of harmful pollutants from air or water.

Rational use and protection of water resources remain one of the world's environmental problems. The solution largely depends on the treatment of wastewater from human activities in the industrial sector [4]. It is especially important to control the content of heavy metals and liquid radioactive wastes because even at low concentrations, they are able to bind the organic molecules and penetrate the human body and living organisms, which could be the cause of physiological disorders and other diseases [5, 6].

Since the discovery of carbon nanotubes (CNTs) by Iijima in 1991 [7], a present investigation of their individual properties and application possibilities as a part of nanocomposites and hybrid materials has begun [8]. The use of CNTs and materials based on them as sorbents is obvious, due to the developed specific surface area, heat resistance, hydrophobicity, and mechanical strength [9].

Development of the carbon nanomaterials has led to appearance of different morphological and variety structure forms of carbon [10]. Among them, carbon nanofibers (CNFs) should be mentioned especially. CNFs belong to sp^2-hybridized filamentary carbon nanomaterials, but differ from CNTs since they do not have an internal hollow channel. The structure and morphology are very diverse: graphene layers can be oriented perpendicular to the fiber axis or at a variable angle [10–12]. The most well-known structures of CNF are "stack of coins" (or plane–parallel, "stacked"); "herringbone" (or a stack of cones, "fishbone", and coaxial–conical); "stack of cups" (or "lampshades"); "feathery" (highly disordered) [8, 10, 11]. Also, there are amorphous CNFs, which exhibit high adsorption capacity [12]. Their length is several micrometers, and the diameter is from tens to 200 nanometers [8, 10]. Both the exact morphology and secondary structure of CNF depend on the reaction (catalytic chemical vapor deposition) conditions, carbon source used, and composition of the catalyst [13–15]. Also worth noting is that they are generally significantly cheaper than the CNTs.

The study of CNFs has not received such a wide resonance as CNTs that allows the CNF-based hybrid materials to be considered as a unique object of research. On the other hand, it is well known that both the reactivity of carbon and the possibility of the formation of hybrid materials or nanocomposites can be significantly improved by functionalization of the CNF surface, since they are unique in that their entire surface can be activated [10].

Among the variety of adsorbents, nanosized metal oxides (NMO) due to the large specific surface area, mesoporous structure, and the ability to ion exchange are considered as a promising material for the removal of heavy metals from aqueous systems. Thereby, such types of nanosized particles have high capacity and selectivity [16–20]. In comparison with organic resins, these materials are much more preferable in terms of thermal, mechanical, and radiation resistance [21]. However, since the size of metal oxides decreases from the micrometer level to the nanometer level, an increase in surface energy inevitably leads to a stability decrease. Consequently, NMOs tend to agglomerate due to Van der Waals forces or other kinds of interactions, and the high capacity and selectivity of NMOs will be significantly reduced or even lost. From this point of view, the usability of NMOs under real conditions of wastewater treatment can be enhanced by supporting them on a porous substrate and thus obtaining composite adsorbents with new unique properties [16].

In this paper, hybrid materials based on CNFs with supported nanosized metal oxides Fe_2O_3 and TiO_2 were synthesized. The resulting hybrids were characterized and examined toward extraction of Sr^{2+}, Cs^{+}, and Ba^{2+} ions from the aqueous solutions.

2 Experimental

2.1 Materials and methods

Carbon nanofibers were obtained as described elsewhere [22]. Catalytic chemical vapor deposition was performed at 700 °C using propane–butane mixture as a carbon source and Ni–Cu/Al$(OH)_3$ as a catalyst. The catalyst was synthesized by a method of mechanochemical activation. The resulting CNFs possess a pore volume of 0.43 cm^3/g and a specific surface area of 313 m^2/g.

CNFs were functionalized as follows: 0.1 g of CNFs were added to 30 mL of a 1:1 mixture of concentrated HCl (37 wt.%) and HNO_3 (65 wt.%), and were boiled for 2 h.

Then they were washed with deionized water (until achieving a neutral pH of the water) to remove the acids and dried at 110 °C. Due to this process, the catalyst particles are converted into soluble salts and removed from the system, as well as carboxyl and hydroxyl bonds formed on the surface of nanofibers, which are involved in the formation of hybrid materials. The oxidized CNFs were used in the experiments.

Hydrosol of Fe (III) hydroxide was synthesized according to the Krekke's method, which is based on the endothermic reaction of hydrolysis of a soluble iron (III) salt:

$$FeCl_3 + 3H_2O = Fe(OH)_3 + 3HCl$$

To this end, 7 ml of an iron (III) chloride solution ($\omega(FeCl_3) = 2\%$) was added slowly to 40 ml of distilled water heated to boil, the mixture was brought to the boil, and then cooled to room temperature. As a result, a red–brown iron (III) hydroxide sol was formed, the micelle of which can be written as $\{m[Fe(OH)_3]nFe^{3+}3(n–x)Cl^-\}^{3x+}3x\ Cl^-$.

Hydrolytic process of the synthesis of nanosized titanium dioxide was prepared according to the reaction

$$Ti(OC_3H_7)_4 + (x+2)H_2O = TiO_2{\cdot}(xH_2O) + 4C_3H_7OH$$

To that end, 0.35 ml of concentrated HNO_3 was added to 50 ml of distilled water. The resulting solution was heated to 70 °C with a magnetic stirrer turned on. When the temperature reached 65 °C, a solution was prepared: in 6 ml of isopropanol, 8 ml of titanium isopropoxide was added. Upon reaching 70 °C, a solution of isopropoxide was poured into it. After 80 °C, the solution was kept for 1 h with constant stirring without the heating. The sol of titanium dioxide was prepared for 5 days.

Hybrid materials were synthesized by ex situ method in two mass ratios, CNF:MeOx = 10:1 and 1:1. Oxidized CNFs were placed in the corresponding sol. The solutions were homogenized at room temperature using a magnetic stirrer overnight. The impregnated CNFs were separated from the solution by dispersion medium filtration and then dried at 110 °C for 2 h.

2.2 Characterization technique

CNFs were investigated by a scanning electron microscopy (Tescan Vega 3 SBH, Czech Republic, detector of secondary electrons). Particle size distribution was received by dynamic light scattering, and zeta potential by electrophoretic light-scattering method using Photocor Compact – Z, Russia.

The structure and microstructure of the powders were examined by a high-resolution transmission electron microscopy (HRTEM) on a JEM-2010 electron microscope (JEOL, Japan), at an accelerating voltage of 200 kV and point-to-point resolution of 0.14 nm. Prior to electron-microscopic examination, the particles were immersed in ethanol and deposited onto porous carbon substrates (hole diameter about 1 μm) secured on copper grids.

Samples were studied using Raman spectroscopy on a LabRam HR800 high-resolution Raman spectrometer (Horiba Jobin Yvon, Japan) using an integrated He–Ne laser with a power of 0.2, 2 mW and an excitation radiation wavelength of 632.8 nm. In the process of recording the spectra, the spectrometer grating was 600 W/mm, the confocal orifice size was 300 μm, and the slit was 100 μm (Objective x50—laser spot 1.5 μm, size of the analyzed region 5 μm). The accumulation time of the signal ranged from 1 to 10 s, the number of measurements in one section of the spectral range varied from 1 to 10 times. The spectra were recorded at room temperature.

XRD measurements were performed on the X-ray diffractometer SHIMADZU XRD-6000, Japan. It was operating in the reflection mode with a Cu X-ray target (30 kV, 30 mA), using a step scan mode with a step of 0.05° (2θ) and scan speed of 1° per minute.

The adsorption and textural properties of the samples were estimated from isotherms of low-temperature (77 K) nitrogen physical adsorption–desorption via volumetry on Quantachrome Nova 1200e surface area and porosity analyzer. The specific surface area was determined by the BET method (A_{BET}). Before the analysis, the samples were held in a vacuum for 2 h at 150 °C.

Hybrids were characterized in terms of sorption capacity with respect to stable cations Sr^{2+}, Ba^{2+}, and Cs^+. Aqueous solutions of the mentioned cations are prepared from $SrCO_3$, $BaCl_2$, and CsCl salts to an initial concentration of 1 g/l of cation. pH values of the stock solutions obtained with the use of a pH meter "Expert-001" were 5.59 ± 0.10 (Sr^{2+}), 5.55 ± 0.10 (Ba^{2+}), and 5.56 ± 0.10 (Cs^+). Sorption was carried out as follows: 20 mg of the sample was placed in a polypropylene tube and poured into 10 ml of solution; the ratio of solid and liquid phases was 1:500. The resulting suspension with periodic shaking was kept at a temperature of 20 °C for 24 h (static conditions). After conducting the experiments, the suspension was centrifuged at a rate of 4500 rpm. To reduce losses during sorption on third-party surfaces, an aliquot of the analyzed solution was taken without additional filtration. The determination of the initial and equilibrium concentrations of cations was performed by an atomic emission spectroscopy with inductively coupled plasma on a Vista MPX Rad spectrometer. The sorption capacity of the samples can be calculated using the following equation:

$$q_e = \frac{C_o - C_e}{m} \cdot V$$

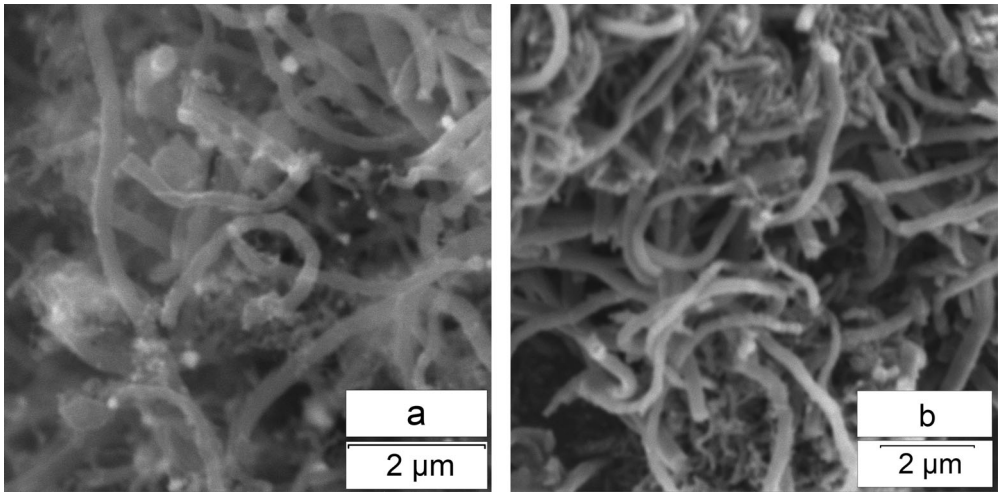

Fig. 1 SEM images of CNF: **a** with catalyst particles (as prepared); **b** without catalyst particles (after acid modification)

where q_e (mg/g) represents the sorption capacity; C_0 (mg/L) and Ce (mg/L) are the initial and equilibrium ion concentrations, respectively. V (L) is the total volume of the suspension, and m (g) is the mass of the adsorbent. All the experiments were performed in duplicate.

The energy of the pair interaction of Fe_2O_3–Fe_2O_3, Fe_2O_3–CNF, TiO_2–TiO_2, and TiO_2–CNF was determined by the DLVO theory, which takes into account electrostatic (U_e) and molecular (U_m) components of pair interaction energy U:

$$U = U_e + U_m.$$

All the calculations have been performed based on the assumption that the NMO form is spherical and the CNF form is cylindrical. The electrostatic component was calculated according to the formula of Ohshim [23, 24]:

$$U_e = \frac{\pi\varepsilon\varepsilon_0 r_1 r_2(\varphi_1^2+\varphi_2^2)}{r_1+r_2}\left\{\frac{2\varphi_1\varphi_2}{\varphi_1^2+\varphi_2^2}\ln\left[\frac{1+\exp\{-\kappa h\}}{1-\exp\{-\kappa h\}}\right] + \ln[1+\exp\{-2\kappa h\}]\right\}$$

where ε is the permittivity of the dispersive medium; ε_0 is the permittivity of vacuum, F/m; r_i are particle radii, m; φ_i are the potentials of the interacting particles, V; κ is the Debye parameter, m^{-1}; and h is the distance between the surfaces of the particles, m.

The molecular attraction energy (U_m) of the particles was calculated by the equation [25]

$$U_m = -\frac{A}{6}\left\{\frac{2r_1r_2}{h^2+2r_1h+2r_2h}+\frac{2r_1r_2}{h^2+2r_1h+2r_2h+4r_1r_2} + \ln\frac{h^2+2r_1h+2r_2h}{h^2+2r_1h+2r_2h+4r_1r_2}\right\}$$

where A is the Hamaker constant for particles interacting through a layer of water. For Fe_2O_3 particles, the value of the constant A_{131} was taken as $3.4\cdot10^{-20}$ J [26], for TiO_2—$2.5\cdot10^{-20}$ J [26], and for CNFs 9.39 10^{-21} J [27]. When calculating the pairwise interaction energy of MeO_x–CNF, the A_{132} value was determined by the equation

$$A_{132} = \left(\sqrt{A_{11}}-\sqrt{A_{33}}\right)\cdot\left(\sqrt{A_{22}}-\sqrt{A_{33}}\right),$$

where A_{11}, A_{22}, and A_{33} are the Hamaker constant for Fe_2O_3 particles [28], TiO_2 [26], CNFs [27], and water [23].

3 Results and discussion

3.1 Characterization of hybrid materials

Figure 1 shows the SEM images of CNFs before and after acid modification. As can be observed, the materials are represented by fibers of up to 10 μm in length and 100–200 nm in diameter, twisted in agglomerates.

Figure 2 shows particle size distribution of hybrid materials, CNFs, and sols of metal oxide NPs. As can be seen, the hydrodynamic diameter of Fe_2O_3 NPs is about 9 nm, and that of TiO_2 NPs is 24 nm. Suspension of CNFs in deionized water shows a maximum intensity at 220 nm. Hybrid CNF/TiO_2 (mass ratio 10:1) has a hydrodynamic diameter of about 230 nm, CNF/Fe_2O_3 (mass ratio 10:1)—150 nm.

Figure 3 shows the HRTEM images of CNF/TiO_2 and CNF/Fe_2O_3 hybrid materials, with a mass ratio of 10:1. It is evident that in both the cases, the metal oxide NPs are uniformly distributed along the carbon nanofiber.

The results of calculation by DLVO theory on the pair interaction energies of the particles are shown in Fig. 4. As

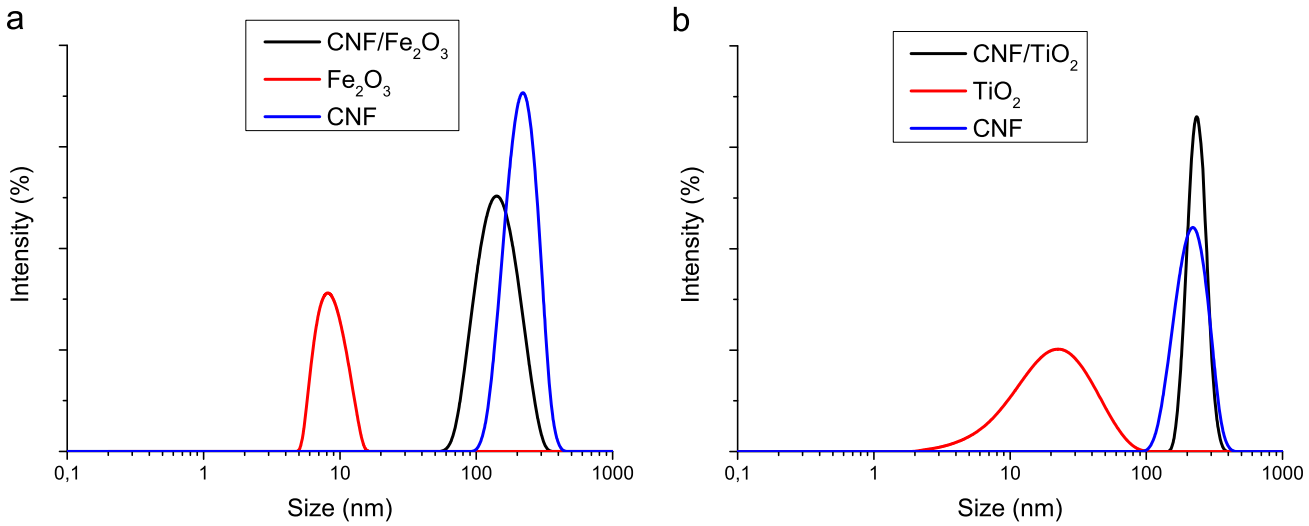

Fig. 2 Particle size distribution of the samples: **a** a system with iron (III) oxide, **b** a system with titanium dioxide

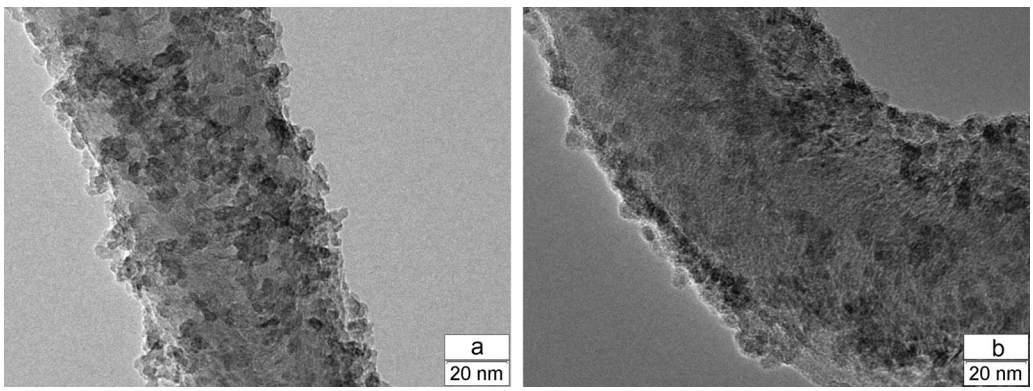

Fig. 3 HRTEM images of **a** CNF/TiO_2 (mass ratio 10:1), **b** CNF/Fe_2O_3 (mass ratio 10:1) hybrid systems

can be seen from the given potential curves, a potential barrier that prevents the particles from approaching each other and from coagulation occurs when particles of the same nature, i.e., CNF–CNF, TiO_2–TiO_2, or Fe_2O_3–Fe_2O_3, interact. The potential barrier height of CNF is higher than that for iron oxide. When oppositely charged Fe_2O_3 particles and CNF interact with each other, the attractive forces prevail at all the distances. The value of the potential barrier decreases in the following order: $Fe_2O_3 > TiO_2 >$ CNF. In general, the energy of attraction between Fe_2O_3 particles and CNF is greater than that between TiO_2 and CNF. Thus, the rates of adsorption and coagulation are higher with the interaction of Fe_2O_3 particles and CNF.

The characteristics of the Raman spectra of the CNF of the initial samples were compared with hybrid materials (mass ratio 10:1). The results of the comparison became a proof of statement that the observed parameters of the spectra, such as the position of the bands, the intensity of

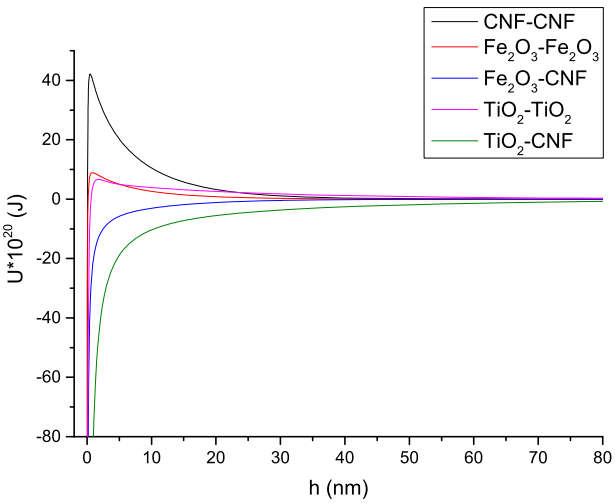

Fig. 4 The dependence of the interaction energies on the distance between the particles

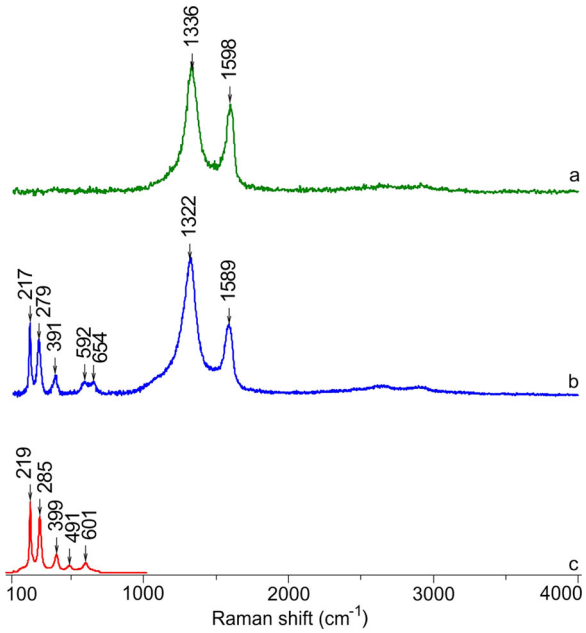

Fig. 5 Raman spectra for the CNF/Fe_2O_3 hybrid sample: **a** laser power 0.2 mW; **b** 20 mW; **c** reference spectrum of the red ocher (Spectral ID Database)

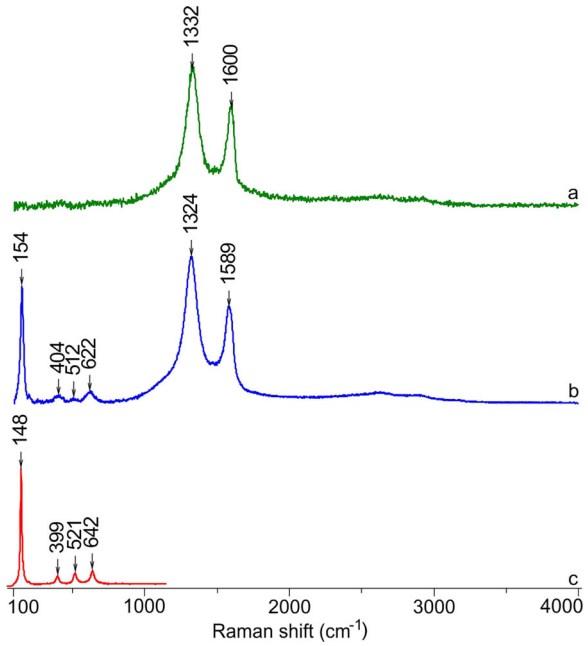

Fig. 6 Raman spectra for the CNF/TiO_2 sample: **a** laser power 0.2 mW; **b** 20 mW; **c** reference spectrum of anatase (Database rruff.info)

the bands of the first and second order vary within the limits of error. Those visible differences in the structure of the CNFs by the method of Raman spectroscopy were not found.

In the Raman spectra for the CNF/Fe_2O_3 hybrid sample with minimal laser exposure (laser power was 0.2 mW), the D-band (position 1336 cm^{-1} is clearly distinguished, its full width at half maximum or FWHM is 100 cm^{-1}), and G-band (position 1598 cm^{-1}, FWHM = 59) are presented. The bands of the second order are weakly expressed (Fig. 5a). As the laser power increases during registration of the Raman spectra, the D- and G-bands of the CNF are shifted, which is associated with the sample heating, and the bands at 217, 279, 391, 592, and 654 cm^{-1} begin to appear (Fig. 5b). It is noteworthy that these bands are characteristic for the mineral red ocher (Fig. 5c). During the temperature exposure, a partial burnout of the CNF most likely occurs, and the signal from the red ocher contributes to the analyzed spectrum.

A similar picture was observed for CNF/TiO_2 samples. With minimal laser exposure (laser power was 0.2 mW), the D-band (position 1332 cm^{-1}, its full width at half maximum or FWHM is 100 cm^{-1}) and the G-band (position 1600 cm^{-1}, FWHM = 53) are presented. Second-order bands are weakly expressed (Fig. 6a). As the laser power increases, the D- and G-bands of the CNF are shifted, which is associated with the sample heating during the registration of the Raman spectra, and the bands at 154, 404, 512, and 622 cm^{-1} characteristic of the anatase mineral (Fig. 6c) have appeared (Fig. 6b). A slight shift of the bands and the broadening of the lines in the studied samples, in contrast to the reference ones, may be associated with the disordering of the structure. Further, during the temperature exposure, a partial burnout of the CNF most likely occurs, and the signal from anatase also contributes to the analyzed spectrum.

XRD measurements, shown in Fig. 7, represent that the crystal structure of the hybrids is primarily determined by the crystal structure of the starting components. The diffraction pattern of the Fe_2O_3 sol dried at 110 °C is characterized by the peaks of akaganeite (β-FeOOH). The intense diffraction peak of CNF/Fe_2O_3 (mass ratio 10:1) corresponds to graphite. All the diffraction peaks in the XRD pattern of the hybrid CNF/TiO_2 sample (mass ratio 10:1) and of the TiO_2 can be perfectly assigned to the anatase phase. The crystalline structure was determined using the AMCSD database (for anatase _database_code_amcsd 0010735, for akaganeite _database_code_amcsd 0001349).

Nitrogen adsorption–desorption isotherms and pore size of the CNFs, hybrids, TiO_2, and Fe_2O_3 are shown in Fig. 8. The isotherms and pore size of hybrids determined by the structure of the fibers refer to the type IV (IUPAC classification). They exhibit combined H2 and H3 hysteresis loops. These features indicate the existence of a mesoporous structure and slit-like pores. The Brunauer–Emmett–Teller (BET) surface areas of the CNFs, CNF/Fe_2O_3 (10:1), and CNF/TiO_2 (10:1) samples were calculated to be 161 m^2/g, 123 m^2/g, and 131 m^2/g, correspondingly.

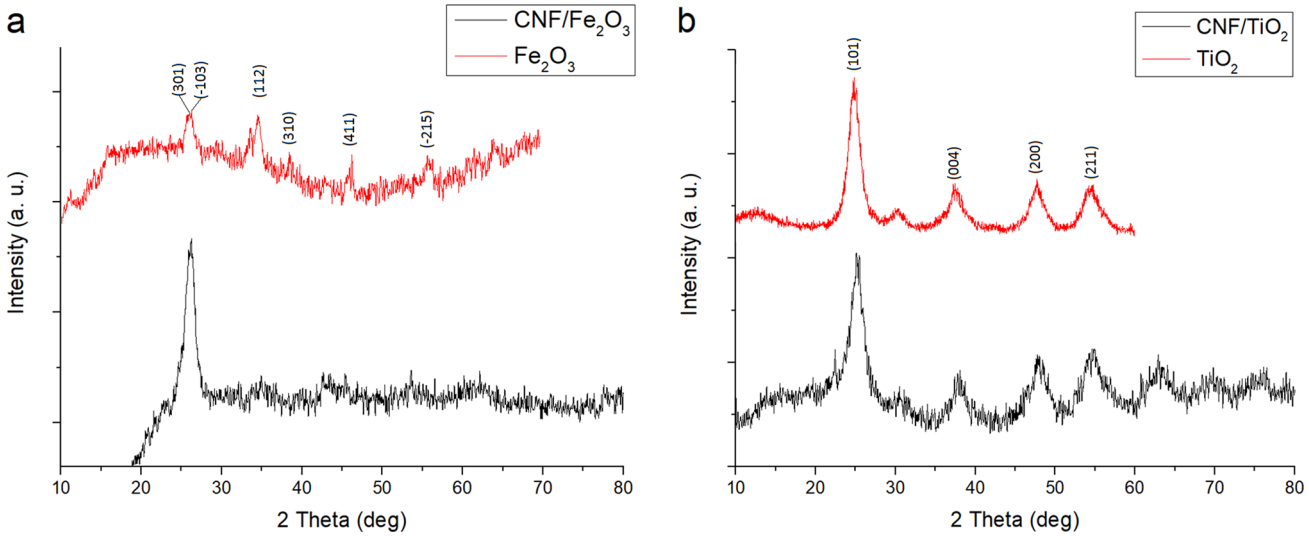

Fig. 7 XRD analysis of hybrid materials: **a** CNF/Fe_2O_3 (mass ratio 10:1); **b** CNF/TiO_2 (mass ratio 10:1)

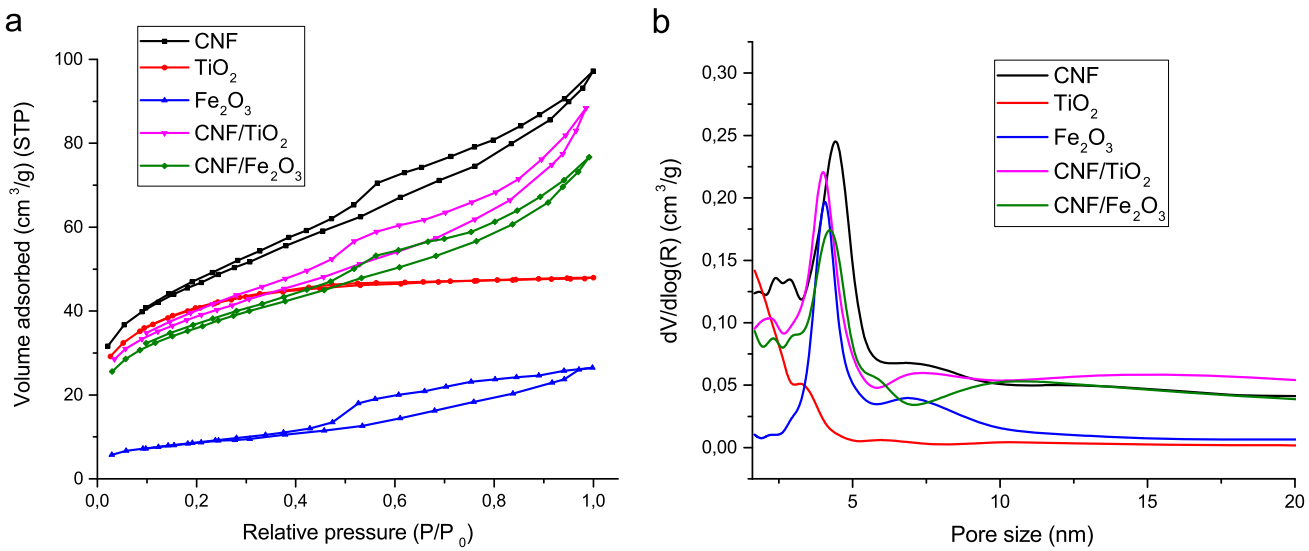

Fig. 8 Isotherms of low-temperature nitrogen adsorption–desorption **a** and pore size distributions **b**, calculated using the BJH method

Table 1 pH values of the solutions after the sorption of Sr^{2+} ions

Sample	pH
CNF	3.5
CNF/Fe_2O_3 (10:1)	3.3
CNF/Fe_2O_3 (1:1)	2.7
CNF/TiO_2 (10:1)	3.6
CNF/TiO_2 (1:1)	3.2
TiO_2	2.7
Fe_2O_3	2.6

Titanium dioxide isotherm is of the type I, which indicates the predominant presence of micropores, BET surface area—148 m^2/g. Iron (III) oxide isotherm refers to the type IV hysteresis loop combined with H2 and H4 types, BET surface area is 29 m^2/g.

3.2 Sorption properties

The pH values of Sr^{2+} solutions after interaction with the studied samples were measured in advance. The solid-to-liquid ratio was 1:500 (10 mg to 5 ml), and the contact time

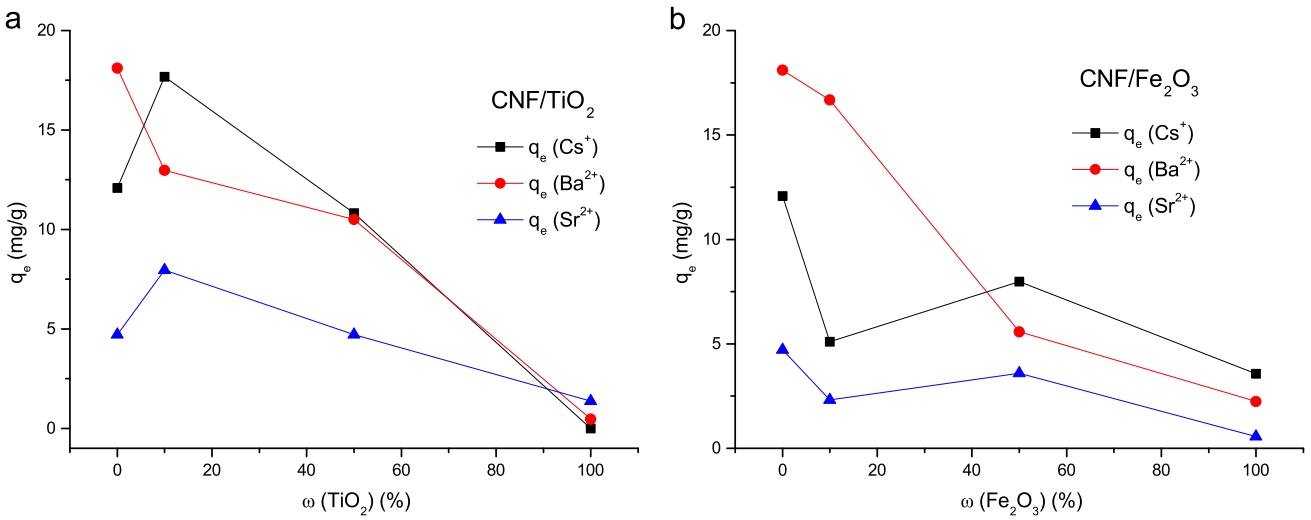

Fig. 9 Sorption capacity for CNF/TiO_2 **a** and CNF/Fe_2O_3 **b** hybrids

of the solution with the sample was 5 min. When a complex with Sr^{2+} ions is formed, a proton is displaced from each reagent molecule; therefore, after the sorption, a decrease in the pH of the solution is observed (Table 1). In this case, the mechanism of chemisorption is most likely to be implemented.

Figure 9a illustrates data on sorption capacity for the CNF/TiO_2. The growth of the sorption capacity for CNF/TiO_2 (10:1) can be explained by the fixation mechanism of TiO_2. There is a blocking of free protons, which can be seen when measuring pH.

In hybrids CNF/Fe_2O_3, a gradual decrease in the sorption capacity is observed with increasing iron (III) oxide content (Fig. 9b). This can be explained by the fact that iron (III) oxide has a less developed specific surface area.

As a result of the research, it was found that for a CNF with deposited TiO_2 with a mass ratio of 10:1, a synergistic effect is observed, manifested in an increase in the sorption capacity.

4 Conclusion

Hybrid CNF/Fe_2O_3 and CNF/TiO_2 materials were synthesized by ex situ method and characterized by a number of techniques (SEM, DLS, TEM, Raman, XRD, BET, and DLVO theory). TEM images showed coaxial coating and a uniform distribution of MeOx NPs on the CNF surface. Raman spectroscopy results demonstrated the electrostatic attraction between components without the formation of covalent bonds. Sorption property results revealed the synergistic effect of the hybrid CNF/TiO_2 (10:1) in relation to Cs^+ and Sr^{2+}, which demonstrates its prospects to be used as an effective adsorbent.

Acknowledgements This research was supported by a grant from the Russian Foundation for Basic Research (project no. 18-29-19053_mk).

Compliance with ethical standards

Conflict of interest The authors declare that they have no conflict of interest.

References

1. Krivoshapkin PV, Mishakov IV, Vedyagin AA, Bauman YI, Krivoshapkina EF (2017) Synthesis and characterization of carbon/ceramic composite materials for environmental applications. Compos Commun 6:17–19. https://doi.org/10.1016/j.coco.2017.08.001
2. Shearer CJ, Cherevan A, Eder D (2014) Application and future challenges of functional nanocarbon hybrids. Adv Mater 26:2295–2318. https://doi.org/10.1002/adma.201305254
3. Vilatela JJ, Eder D (2012) Nanocarbon composites and hybrids in sustainability: a review. ChemSusChem 5:456–478. https://doi.org/10.1002/cssc.201100536
4. Burakov AE, Galunin EV, Burakova IV, Kucherova AE, Agarwal S, Tkachev AG, Gupta VK (2018) Adsorption of heavy metals on conventional and nanostructured materials for wastewater treatment purposes: a review. Ecotoxicol Environ Saf 148:702–712. https://doi.org/10.1016/j.ecoenv.2017.11.034
5. Fan HT, Su ZJ, Fan XL, Guo MM, Wang J, Gao S, Sun T (2012) Sol–gel derived organic–inorganic hybrid sorbent for removal of Pb^{2+}, Cd^{2+} and Cu^{2+} from aqueous solution. J Sol-Gel Sci Technol 64:418–426. https://doi.org/10.1007/s10971-012-2872-x

6. Khalili SS, Dehghani H, Afrooz M (2018) New porphyrin-doped silica monolith: an effective adsorbent for heavy metal ions in aqueous solution. J Sol-Gel Sci Technol 85:290–301. https://doi.org/10.1007/s10971-017-4548-z
7. Liu X, Wang M, Zhang S, Pan B (2013) Application potential of carbon nanotubes in water treatment: a review. JES 25:1263–1280. https://doi.org/10.1016/S1001-0742(12)60161-2
8. Huang J, Liu Y, You T (2010) Carbon nanofiber based electrochemical biosensors: a review. Anal Meth 3:202–211. https://doi.org/10.1039/B9AY00312F
9. Postnov VN, Rodinkov OV, Moskvin LN, Novikov AG, Bugaichenko AS, Krokhina OA (2016) From carbon nanostructures to high-performance sorbents for chromatographic separation and preconcentration. Russ Chem Rev 85:115–138. https://doi.org/10.1070/RCR4551
10. Vamvakaki V, Tsagaraki K, Chaniotakis N (2006) Carbon nanofiber-based glucose biosensor. Anal Chem 15:5538–5542. https://doi.org/10.1021/ac060551t
11. Poveda RL, Gupta N (2016) Carbon nanofibers: structure and fabrication. Carbon Nanofiber Reinforced Polymer Composites. Springer, Cham
12. Rakov EG (2006) Nanotubes and fullerenes. Logos, Moscow
13. Mishakov IV, Buyanov RA, Zaikovskii VI, Strel'tsov IA, Vedyagin AA (2008) Catalytic synthesis of nanosized feathery carbon structures via the carbide cycle mechanism. Kinet Catal 49:868–872. https://doi.org/10.1134/S0023158408060116
14. Mishakov IV, Bauman YI, Streltsov IA, Korneev DV, Vinokurova OB, Vedyagin AA (2016) The regularities of the formation of carbon nanostructures from hydrocarbons based on the composition of the reaction mixture. Resource-Efficient Technologies 2:61–67. https://doi.org/10.1016/j.reffit.2016.06.004
15. Krasnikova IV, Mishakov IV, Bauman YI, Karnaukhov TM, Vedyagin AA (2017) Preparation of NiO-CuO-MgO fine powders by ultrasonic spray pyrolysis for carbon nanofibers synthesis. Chem Phys Lett 684:36–38. https://doi.org/10.1016/j.cplett.2017.06.036
16. Hua M, Zhang S, Pan B, Zhang W, Lv L, Zhang Q (2012) Heavy metal removal from water/wastewater by nanosized metal oxides: A review. J Hazard Mat. 211–212:317–331. https://doi.org/10.1016/j.jhazmat.2011.10.016
17. Topel SD, Legaria EP, Tiseanu C, Rocha J, Nedelec JM, Kessler VG, Seisenbaeva GA (2014) Hybrid silica nanoparticles for sequestration and luminescence detection of trivalent rare-earth ions (Dy3+ and Nd3+) in solution. J Nanopart Res 16:2783. https://doi.org/10.1007/s11051-014-2783-6
18. Ivanets AI, Srivastava V, Roshchina MY, Sillanpää M, Prozorovich VG, Pankov VV (2018) Magnesium ferrite nanoparticles as a magnetic sorbent for the removal of Mn2+, Co2+, Ni2+ and Cu2+ from aqueous solution. Ceram Int 44:9097–9104. https://doi.org/10.1016/j.ceramint.2018.02.117
19. Anastasova EI, Ivanovski V, Fakhardo AF, Lepeshkin AI, Omar S, Drozdov AS, Vinogradov VV (2017) A pure magnetite hydrogel: synthesis, properties and possible applications. Soft matter 13:8651–8660. https://doi.org/10.1039/C7SM01702B
20. Mikhaylov VI, Krivoshapkina EF, Trigub AL, Stalugin VV, Krivoshapkin PV (2018) Detection and adsorption of Cr (VI) ions by Mesoporous Fe-Alumina Films. ACS Sustainable Chemistry & Engineering 6:9283–9292. https://doi.org/10.1021/acssuschemeng.8b01598
21. Zemskova LA (2009) Modified carbon fibers: sorbents, electrode materials, catalysts. Vestn LVO RAN 2:39–52
22. Strel'tsov IA, Vinokurova OB, Tokareva IV, Mishakov IV, Isupov VP, Shubin YV, Vedyagin AA (2014) Effect of the nature of a textural promoter on the catalytic properties of a nickel-copper catalyst for hydrocarbon processing in the production of carbon nanofibers. Catalysis in Industry 6:176–181. https://doi.org/10.1134/S2070050414030131
23. Khamova TV, Shilova OA, Golikova EV (2006) Investigation of the structuring in the Sol-Gel systems based on tetraethoxysilane. Glass Phys Chem 32:448–459. https://doi.org/10.1134/S1087659606040092
24. Ohshima H, Healy TW, White LR (1982) Improvement on the Hogg—Healy—Fuerstenau formulas for the interaction of dissimilar double layers: I. Second and third approximations for moderate potentials. J Colloid Interface Sci 89:484–493. https://doi.org/10.1016/0021-9797(82)90199-0
25. Elimelech M, Gregory J, Jia X, Williams RA (1995) Particle deposition and aggregation: measurement, modelling and simulationButterworth-Heinemann, Woburn, MA, pp 443
26. Lu S, Pugh RJ, Forssberg KSE (2005) Interfacial separation of particles. Elsevier, Amsterdam, xii, 694. 22
27. Shi W, Li S, Chen B, Wang C, Sun W (2017) Effects of Fe2O3 and ZnO nanoparticles on 17β-estradiol adsorption to carbon nanotubes. Chem Eng J 326:1134–1144. https://doi.org/10.1016/j.cej.2017.05.007
28. Israelachvili JN (2011) Intermolecular and surface forces. Academic Press, Burlington, MA